scientific reports

Check for updates

OPEN

Actin cytoskeleton dynamics affect replication of human Metapneumovirus

Pamela Elizabeth Rodríguez[1,4], Pedro Ignacio Gil[2,4], Jorge Augusto Cámara[1], Alicia Cámara[1] & María Gabriela Paglini[2,3]✉

Human Metapneumovirus (hMPV) is a leading cause of viral respiratory infection with clinical and epidemiological relevance in pediatric, immunocompromised, and elderly populations. Little is known about hMPV in vitro replication processes and their relationship with cellular structures such as the cytoskeleton. Our goal was to evaluate the role of the actin cytoskeleton in hMPV replication at different stages of viral growth. hMPV was isolated in Vero cells from a clinical sample and identified as A_2 genotype. The cytopathic effect was detected by the appearance of cell rounding and refractory cell clusters. The growth curve showed that viral replication maximum level was between 48 and 72 hpi. The highest percentage of infected cells and intracellular hMPV-protein were detected at the early stages of the replication cycle. Disruption of actin microfilaments with Cytochalasin D during the early events provoked an increase in intracellular and extracellular viruses. We demonstrate that the early phase of the hMPV curve is crucial for viral replication; and the disruption of microfilaments during this time increases both viral protein expression and release of viruses to the extracellular space. This study aims to elucidate wild-type hMPV growth kinetics, providing new insights into the role of actin cytoskeleton in viral replication mechanisms.

Keywords Virus isolation, Replication cycle, Actin filaments, Cytochalasin D, Respiratory disease.

Two members of the *Pneumoviridae* family[1] human Metapneumovirus (hMPV) and respiratory syncytial virus (RSV), cause severe respiratory diseases in infants, immunocompromised and older adults[2]. Currently, for RSV, a bivalent prefusion F vaccine was approved for use during pregnancy in 2023 to protect infants from severe RSV illness during their early months of life[3]. However, there is no licensed vaccine or approved antiviral therapy available for hMPV.

HMPV is an enveloped negative-stranded RNA virus with a non-segmented genome composed of eight genes encoding for nine proteins[4]. hMPV is classified into two major genetic lineages, type A (subtypes A1, A2a, A2b1 and A2b2) and type B (subtypes B1 and B2)[2,5].

Since the discovery of hMPV[5], several approaches for its in vitro isolation have been followed. Viral adaptation and spread in cell cultures are difficult since both require high viral loads and successive blind passages of about 14–21 days to visualize the cytopathic effect (CPE), characterized by changes in cell morphology or by the formation of syncytia[6,7].

Viruses from diverse families have evolved to hijack components of the host cytoskeleton—microtubules and microfilaments (MFLs)—to facilitate multiple stages of their life cycle, including attachment, internalization, intracellular trafficking, replication complex formation, assembly, and spread[8]. MFLs remodeling, regulated by a dynamic balance between actin polymerization and depolymerization, supports membrane ruffling, vesicle movement, and formation of cellular protrusions, all of which can be co-opted by viruses to enhance infectivity, a strategy widely exploited across viral families, including respiratory viruses[9]. In this sense, it has been shown that actin cytoskeleton components are essential cofactors for RSV replication, spread, and morphogenesis[10–13]. In the case of hMPV, infection induces prominent reorganization of F-actin, including the formation of branched

[1]Laboratory of Influenza and other Respiratory Viruses, Virology Institute "Dr. J. M. Vanella", Facultad de Ciencias Médicas, Universidad Nacional de Córdoba, Córdoba, Córdoba, Argentina. [2]Laboratory of Cell Biology of Viral Infection, Virology Institute "Dr. J. M. Vanella". Facultad de Ciencias Médicas, Universidad Nacional de Córdoba, Enfermera Gordillo s/n. Ciudad Universitaria, Córdoba, Córdoba 5000, Argentina. [3]Laboratory of Neurophysiology, Instituto de Investigación Médica Mercedes y Martín Ferreyra, INIMEC-CONICET, Universidad Nacional de Córdoba, Córdoba, Argentina. [4]Pamela Elizabeth Rodríguez and Pedro Ignacio Gil contributed equally to this work. ✉email: gpaglini@immf.uncor.edu

filament networks and intercellular extensions. The viral phosphoprotein co-localizes with actin within these structures, which has been shown to be critical for direct cell-to-cell spread and viral morphogenesis[14]. Moreover, previous studies from our laboratory demonstrated that the disruption of the actin cytoskeleton during early stage of Pixuna virus (PIXV) replication, increased the extracellular viral yields, probably promoting endocytosis and thus increasing the entry of viral particles[15].

Despite hMPV's importance as an etiological agent of respiratory pathologies, the mechanisms of interaction between virus and host cell to secure infection remain largely unexplored. We examined the role of MFLs in hMPV replication at different stages of viral growth, under in vitro conditions using Vero cells. By analyzing the replication curve and subcellular distribution of viral proteins at various time points post-entry, we found that early actin depolymerization by Cytochalasin D (CytD), which inhibits filament elongation by capping the barbed ends[16], increases cytoplasmic viral protein expression and promotes viral release into extracellular space.

Understanding the molecular mechanisms governing hMPV replication is essential to elucidate virus-host interactions and provides the basis for identifying potential antiviral targets.

Results

Human Metapneumovirus isolation and identification

Human Metapneumovirus was isolated from NPA of hospitalized children in Cordoba, Argentina, which had previously tested negative for common respiratory viruses such as influenza virus A and B, respiratory syncytial virus (RSV), adenovirus, and parainfluenza virus types 1, 2, and 3[17], thereby minimizing the possibility of co-infection with pathogens that could induce similar cytopathic effects (CPE).

The virus replicated in Vero cells cultures after three blind passages of 21 days each one. The CPE was characterized by cell rounding, detachment, and formation of refractory cell clusters (Fig. 1A). Immunofluorescen (IF) detection confirmed that the CPE was caused by hMPV. The presence of specific hMPV proteins was observed at 4, 7, and 14 dpi located and distributed in the cell cytoplasm presenting a dotted pattern (Fig. 1B). Simultaneously, virus genome detection by nucleic acid amplification assays (RT-PCR) from supernatants of infected cultures collected at 4, 7, and 14 dpi were positive for the amplification of the 199 bp N protein (Fig. 1C),

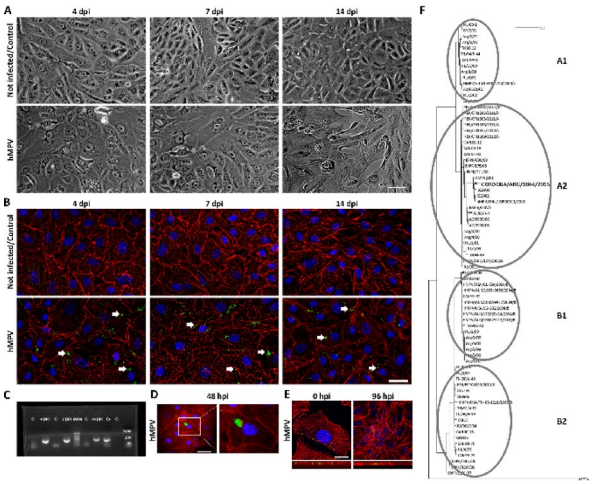


Fig. 1. Human Metapneumovirus (hMPV) isolation and identification. (**A**,**B**) Representative images of uninfected and infected VERO cells with hMPV. (**A**) Images were obtained with phase contrast microscopy at low magnification, showing the viral infection cytopathic effect (CPE), which is visible at 14 d.p.i as cell rounding and shedding. Uninfected cells (top panel) and infected cells (bottom panel) at 4, 7 and 14 days dpi. Scale bar: 20 µm. (**B**) The localization of the hMPV protein was determined using indirect immunofluorescence with specific anti-hMPV antibodies targeting protein F (green-colored). MFLs were labeled with Phalloidin-Rho (red-colored), and nuclei were stained with Hoechst (blue-colored). A temporary sequence of 4 to 14 days in non infected (top panel) and infected cells (bottom panel). White arrows indicate the fluorescent label of the F protein. Scale bar: 20 µm. (**C**) Amplification products (RT-PCR) of the hMPV N protein region (199 bp) by agarose gel electrophoresis. Bands corresponding to culture supernatants of infected cells collected at 4, 7 and 14 dpi and positive controls (C+) are shown. Uninfected cells collected at the same times are included (C-). MPM: molecular weight marker. (**D**) Images obtained with epi-fluorescence microscopy, showing that the hMPV F protein accumulates near the nucleus at 48 hpi. Scale bar: 100 µm. (**E**) Confocal microscopy images where viral proteins are observed at 0 and 96 hpi. The bottom panel shows a transverse optical section where the viral label is evidenced in the cell cytoplasm decorating the MFLs. Scale bar: 20 µm. (**F**) A maximum-likelihood tree (PhyML software) was constructed using a 696 bp region of the fusion (F) gene of hMPV. The GTR + G model was applied with parameters selected by JModelTest 3.7. Branch support was evaluated using 1000 bootstraps pseudoreplicates. A1: strains belonging to hMPV subgroup A1. A2: strains to hMPV subgroup A2. B1: strains to hMPV subgroup B1. B2: strains to hMPV subgroup B2. Avian MPV (aMPV) was used to root the tree. The strain of interest is marked in bold. The scale bar indicates the changes between nucleotides. All data were obteinded from 5 independet experiments.

confirming the presence of hMPV in infected culture. Viral isolation was typified, the Cordoba/ARG/3864/2015 local isolated strain (no: MN117139) was identified as A_2 hMPV and grouped with Canada and The Netherlands prototype strains, and with sequences from Argentina[17,18], Peru, Brazil, United States, China, and Italy (Fig. 1F).

Different subcellular localization of large fluorescent dots were observed several times post-infection (Fig. 1B,D), while confocal microscopy detected small dots between 0 and 96 hpi in areas enriched in actin filaments, below the plasma membrane (Fig. 1E, low panel).

The hMPV replication cycle

To characterize hMPV replication kinetics, we evaluated the production and release of the virus over time (8, 16, 24, 48, 72, and 96 hpi) using qRT-PCR (RNA copies/µl of culture supernatant). RNA copies increased progressively until 72 hpi, peaking at 4961 copies/µl of supernatant (Fig. 2A). The time course of hMPV infection was also studied by IF and viral proteins was quantified as number of fluorescent dots/infected cell (Fig. 2B,D). Interestingly, the number of fluorescent dots/infected cell decreased while the number of copies of RNA/µl of culture supernatant increased. At 72 hpi the maximum extracellular viral yield (4961 copies) corresponded to the minimum number of cytoplasmic dots (2.2 dots), as well as to the lowest percentage of infected cells (32.8%) (Fig. 2C). It is important to highlight that the percentage of infected cells decreased significantly and progressively from 24 hpi until the end of the experiment (Fig. 2C,D).

Taken together, our results demonstrate that the highest percentage of infected cells and intracellular hMPV-protein contents were detected at the early phase of the replication cycle. While the cycle progressed, hMPV immunostaining decreased whereas extracellular viral RNA increased due to the release of the viral progeny.

Actin microfilament perturbation at different viral stages affects hMPV replication

Previous studies highlight the involvement of the cytoskeleton, particularly MFLs, in the entry and replication of numerous viruses[19]. Therefore, we studied the role of MFLs at early and late stages of hMPV infection cycle. For this, disruption of actin polymerization was performed using CytD at different times of hMPV infection. We first determined the participation of MFLs during the entry and at its early stages of hMPV replication. To this end, CytD was applied during virus infection (2 h), during the first 8 hpi and during the first 24 hpi (Fig. 3B).

Treatment with CytD during early replication stages prevented the significant decrease in the number of infected cells, maintaining initial percentage, regardless of drug exposure timing (Fig. 3A,C). Interestingly, CytD treatment during the first 24 hpi, also prevented the dramatic diminution in the percentage of infected cells at 72 hpi (75.3%) compared to control (33.3%) (Fig. 3C). To obtain a quantitative measure of CytD effect on F viral protein expression at the different stages of the replication cycle, we quantified the number of fluorescent dots/infected cell. CytD treatment during infection or during the first 8 hpi significantly increased fluorescent dots/infected cell compared to controls (Fig. 3A,D). Particularly, during the first 8 hpi of treatment a 2 to 2.5 fold increase was observed at both analyzed times (8 hpi and 24 hpi) (Fig. 3A,D). When CytD was applied during

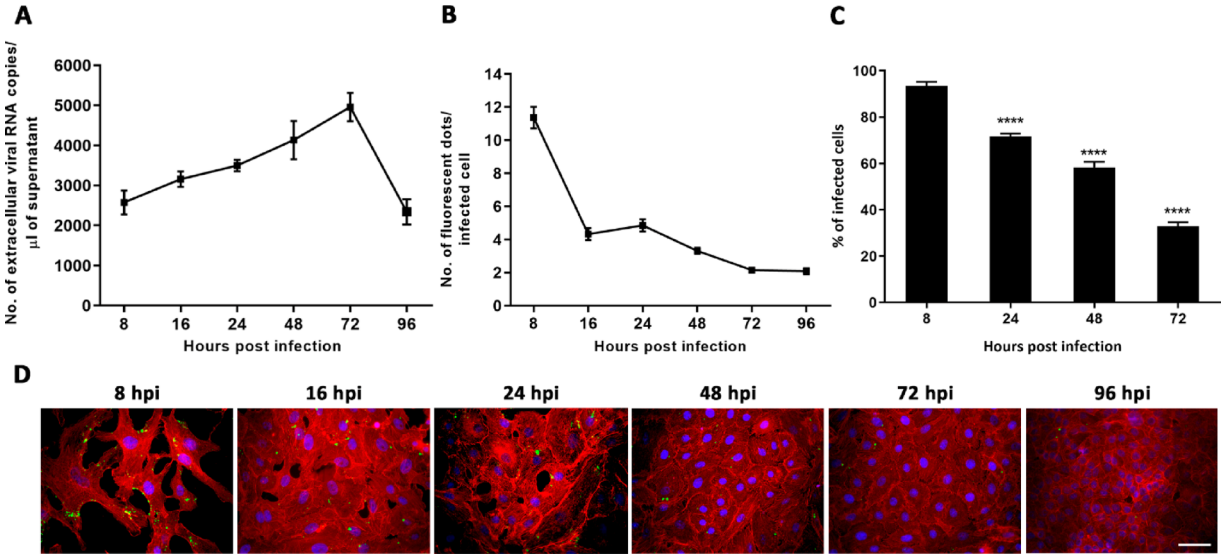


Fig. 2. HMPV viral replication curve. (**A**) Quantification curve of extracellular viral production through the number of copies of viral RNA in the extracellular medium. Quantification was performed at 8, 16, 24, 48, 72 and 96 hpi. (**B**) Quantification of intracellular viral production through the number of fluorescent dots/infected cell (cytoplasmic viral F protein). Quantification was performed at 8, 16, 24, 48, 72 and 96 hpi. (**C**) Percentage of quantified infected cells was determined by the number of cells with or without fluorescent dots at 8, 24, 48, and 72 hpi. (**D**) Representative images of the temporal sequence of infection (0–96 hpi). The hMPV F protein label (green-colored), MFLs (red-colored) and nuclei (Hoechst, blue-colored) are observed. Scale bar: 20 µm. More than 400 cells were screened in each time point. Data represent the mean ± SEM from 3 independent experiments (one-way ANOVA with Tukey test post hoc test). **** <0.0001.

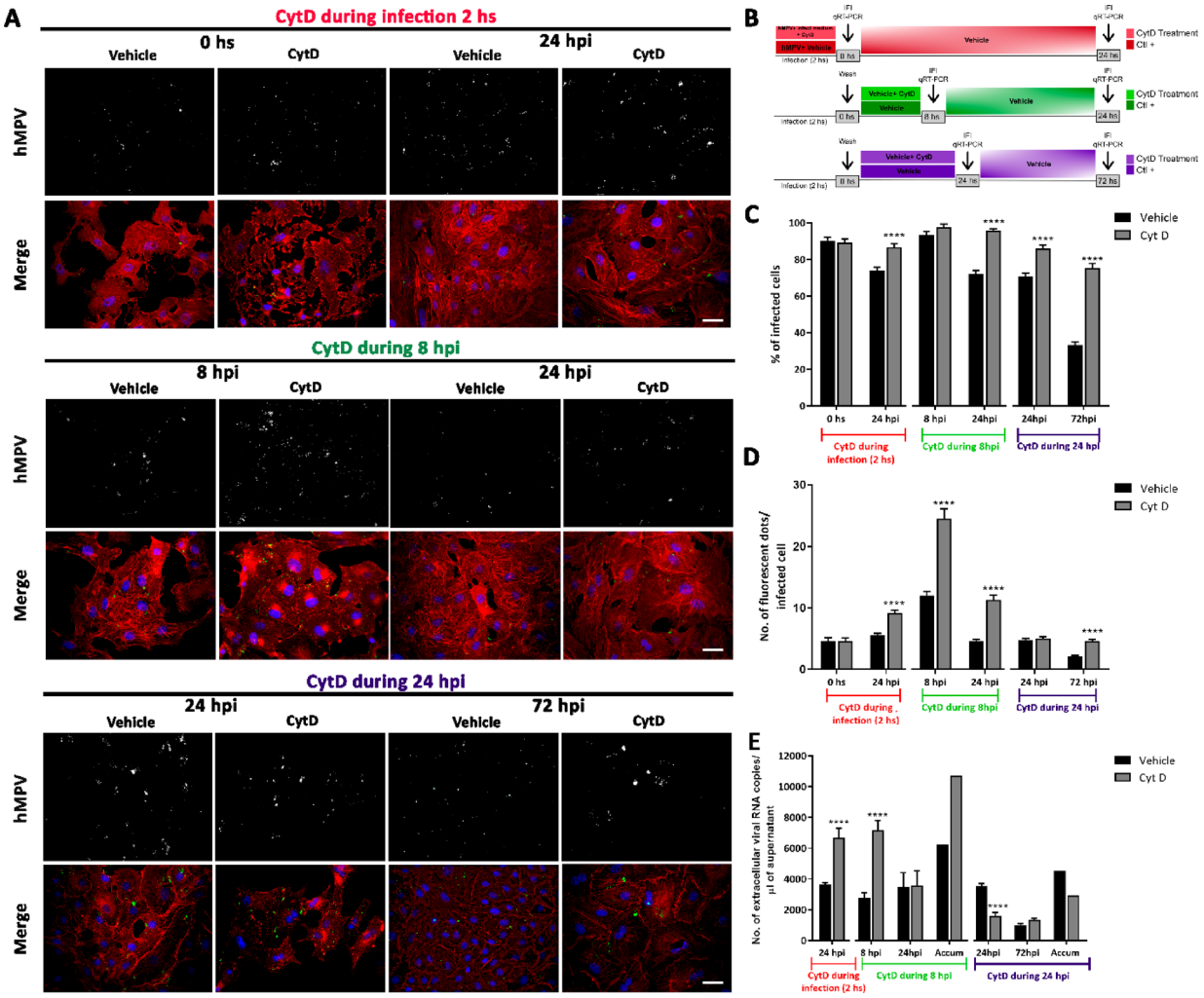


Fig. 3. Effect of disruption of MFLs with CytD at different stages of the viral cycle. (**A**) Images of CytD treatments in hMPV infected cells at different times of the growth curve: CytD during infection (2 h), during 8 hpi and during 24 hpi. Immunofluorescence performed with specific hMPV antibodies anti-protein F (green-colored), MFLs (Phalloidin-Rho, red-colored) and nuclei (Hoechst, blue-colored). (**B**) The scheme illustrates the pharmacological treatment with CytD at different times during the viral replication cycle and the time points of experimental procedures. In red color: cells exposed to vehicle or CytD during the 2 infection hours. In green color: cells exposed to vehicle or CytD throughout the first 8 hpi. In violet color: cells exposed to vehicle or CytD during the first 24 hpi. (**C**) Percentage of infected cells after CytD treatment in relation to vehicle control. CytD treatment during infection (2 h): a significant increase was observed at 24 hpi ($p < 0.0001$). CytD treatment during the first 8 hpi: a significant increase was observed at 24 hpi ($p < 0.0001$). In CytD treatment during first 24 hpi a significant increase was observed both at 24 and 72 hpi (24 hpi: $p < 0.0001$; 72 hpi: $p < 0.0001$). (**D**) Number of fluorescent dots per infected cell in CytD treatments and in controls. CytD treatment during infection (2 h): a significant increase was observed at 24 hpi ($p < 0.0001$). CytD treatment during the first 8 hpi: a significant increase was observed both at 8 and 24 hpi (8 hpi: $p < 0.0001$; 24 hpi: $p < 0.0001$). CytD treatment during the first 24 hpi: a significant increase was observed at 72 hpi ($p < 0.0001$). (**E**) Quantification of extracellular viral RNA. CytD treatment during infection (2 h): a significant increase in RNA copies in the culture supernatant was observed at 24 hpi ($p < 0.0001$). CytD treatment during the first 8 hpi caused a significant increase in RNA copies in culture supernatant at 8 hpi ($p < 0.0001$); this was also observed in the accumulated values (sum of the means of RNA copies at 8 plus 24 hpi). CytD treatment during the first 24 hpi caused a significant decrease in extracellular viral RNA copies ($p < 0.0001$), remaining constant until 72 hpi; this was also observed in the accumulated values (sum of the means of RNA copies at 24 and 72 hpi). Scale bar: 20 µm. More than 400 cells were screened in each case. Data represent the mean ± SEM from 3 independent experiments. Student unpaired *t* test was performed (**** <0.0001).

the first 24 hpi, and quantified at the end of the treatment, no significant differences in fluorescent dots/infected cells was observed compared to control, but prevented viral protein loss at 72 hpi (Fig. 3D). Finally, we quantified viral-RNA copies in culture supernatant to assess extracellular virus yields (Fig. 3E). CytD treatment during the infection significantly increased viral production at 24 hpi. Treatment during the first 8 hpi significantly

increased RNA copies at that time. This effect was also observed in the accumulated values, this value is the sum of the mean of RNA copies values at 8 plus 24 hpi (for vehicle: 6674; CytD treatment: 10,727; see accumulated value at 24 hpi). On the other hand, CytD treatment during the first 24 hpi, caused a significant decrease in extracellular RNA viral copies at 24 hpi, remaining lower up to 72 hpi, as can be observed in the accumulated values (vehicle: 4510; CytD treatment: 2930; see accumulated value at 72 hpi) (Fig. 3E).

In addition, we focused on the late stage of the replication curve and observed that CytD applied during the last 24 hpi (48–72 hpi) caused no changes in the percentage of infected cells, in the number of fluorescent dots/infected cell or in the number of extracellular RNA-viral copies compared to controls (data not shown).

These results underscore the importance of the initial 8 h of hMPV infection for replication, indicating that CytD presence during this period boots viral protein expression in the cell cytoplasm and enhances virus release into extracellular space.

Discussion

In this study we report the first successful isolation of hMPV performed in Vero cell line from a positive clinical sample in Cordoba, Argentina. We identified this local strain and described the replication curve showing that the maximum viral production takes place at 72 hpi. Moreover, we demonstrate that the disruption of MFL at the early stages of infection increases intracellular viral production and the release of viruses into the extracellular space.

The viral isolate was identified as the A_2 hMPV subtype through phylogenetic analysis, consistent with our previous studies of A_2 hMPV subtype circulation in Argentina[17]. Additionally, co-circulation with other genotypes like A_1, B_1, and B_2, has been reported in our country[18]. Genotype predominance varies based on factors like epidemiological year and region, host immunity, viral load, and susceptibility. Competitive replication was observed between hMPV genotype A and B. A recent study by van den Hoogen's group[20] demonstrated that lineage A replicates more efficiently than lineage B in an organoid-derived human bronchial-epithelium model, with increased viral-RNA and infectious virus particles. They also highlight the use of viruses with a history of controlled passage, instead of extensively passaged hMPV strains. These data are important because the A_2 genotype is clinically relevant, as it may cause diseases of varying severity. In studies where verification was possible, genotype A has been associated with severe conditions such as pneumonia and hypoxia, leading to more ICU admissions compared to the other subtypes[21].

In several studies, hMPV replication is limited to certain cell lines, with varied and mild CPE. Isolation of the A_2 hMPV viral strain in this study showed initial CPE signs at the third blind passage, at 14 dpi, characterized by cell rounding and refractive cells clusters, consistent with previous reports[7,22]. Conversely, other authors have described that hMPV can appear as a syncytium[5,6,23], similar to RSV, and this difference may be related to the cell lines that were infected (e.g. LLC-MK2, tMK, MNT-1, A549) or to the viral genotype[24–26]. Numerous authors note the challenge of hMPV isolation and the absence of an obvious CPE[5,24,25,27]. Isolating respiratory viruses from clinical specimens often exhibits low efficiency in vitro due to factors like cell type and virus subtype[22,27–29]. LLC-MK2 and Vero cells are commonly used for all hMPV strains. Although, this study did not compare different cell lines and isolated only the A2 hMPV subtype, efficient viral replication was achieved, consistent with findings by Nao[26] who demonstrated high infectivity with different hMPV strains in VeroE6 and Vero-ATCC cells.

The hMPV replication curve showed an exponential phase between 48 and 72 hpi, with maximum intracellular viral protein concentration at 8 hpi which is consistent with results obtained by other groups. Tollefson[24] described hMPV kinetics in LLC-MK2 cells, with the eclipse phase at 24 hpi and the exponential phase between 48 and 72 hpi with a significant increase in viral titer. El Najjar[14] showed maximum viral production at 72 hpi in BEAS-2B cells, both intra- and extracellularly. Recent studies using recombinant viruses in Vero cells, three-dimensional cultures and organoid-derived bronchial culture have described similar results, both in the CPE caused by the virus and in the replicative cycle[20,21,30]. All these results show that our model of infection in the Vero-CCL cell line with this wild-type virus (A_2 hMPV), despite its isolation difficulties, is very efficient and representative of in vivo infection.

It is known that viruses such as RSV[10] and PIXV[15], among others, take advantage of structures such as the cytoskeleton for entry, replication and exit from the cell. Our study aimed to assess the role of actin cytoskeleton in hMPV replication. For this, we used CytD, known to disrupt actin polymerization. CytD concentration [2.5μM] was effective and consistent with prior studies[14,29] as well as previously in our laboratory with another viral model[15]. The rapid reversible action of CytD facilitated our experimental designs. Intracellularly, CytD not only prevented the decrease in the percentage of hMPV-infected cells (during 2 h of infection, 8 hpi and 24 hpi) but it also caused a significant increase in the number of fluorescent dots/infected cell, indicative of protein accumulations, in all treatments. In line with this, El Najjar[14] postulates that hMPV proteins assembly during early infection does not require actin polymerization. These protein accumulations (fluorescent dots), resembling "inclusion bodies"[31,32] persist despite actin alteration, hindering viral release. Cifuentes-Muñoz[29] note these structures as primary replication sites, particulary at 24 hpi. In *Pneumovirus*, actin polymerization partially aids inclusion body formation[22]. Unlike Cifuentes-Muñoz[29], our early CytD treatment (8 hpi) boosts extracellular viral load, suggesting that MFLs interruption could facilitate viral entry. This represents an increase in intracellular viral load and a decrease in virus release times, compared to the control. Nevertheless, our results are consistent with those of Cifuentes-Muñoz[29] and El Najjar[14] regarding reduced extracellular viral load from 24 hpi, particularly with continuous 24-hour treatment. Several studies suggest that hMPV relies on cell-cell transmission for efficient spread and infection[19,32–34]. Actin disruption may hinder this process, redirecting virions to alternate exit routes and leading to extracellular accumulation. Therefore, actin dynamics is essential for hMPV infection, enabling cell-to-cell spread regardless of the extracellular viral load[14]. This could explain cytoplasmic viral protein accumulation and the decrease of extracellular viral load after 24 hpi CytD exposure.

Given MFLs are involved in viral particle internalization and release[29], it is reasonable to think that short-term disruption of MFLs with CytD would facilitate viral particles internalization. Conversely, prolonged CytD treatment (24 hpi), could prevent the transport of viral proteins and/or nucleocapsid, reducing cytoplasmic accumulation and extracellular viral loading. Despite the years since its discovery, the cell biology of hMPV infection remains poorly understood. This study broadens our knowledge on the isolation and growth curve characterization of a wild-type hMPV obtained from a clinical sample. Furthermore, these findings provide new insights on hMPV infection and the role of actin cytoskeleton in viral replication, enhancing understanding of hMPV internalization and spreading mechanisms.

Methods

Cell culture and virus isolation

Vero cells (ATCC® CCL-81) were grown in Minimum Essential Medium (MEM, GIBCO-BRL®) supplemented with 5–10% fetal bovine serum (FBS, Natocor), and 1% antibiotic-antimycotic (Pen-Strept 100X, GIBCO), at 37 °C and 5% CO_2.

Human Metapneumovirus was isolated from nasopharyngeal aspirates (NPA) of hospitalized children in Córdoba, Argentina. All procedures were complied with the principles outlined by the Declaration of Helsinki and were approved by an Independent Ethics Committee of Hospital de Niños "Santísima Trinidad" (CIEIS) Protocol: 05/2011. The volunteers who donated samples, signed written assent/informed consent and their personal data was kept anonymous. The infection protocol was adapted from Van den Hoogen[5]. The infection medium consisted of MEM supplemented with 0.00125% trypsin (Trypsin Solution 10×, SIGMA®) to allow F-protein cleavage, 0.3% bovine serum albumin (BSA; SIGMA®), and 1% antibiotic-antimycotic solution (Penicillin and Streptomycin 100×, Stabilized, GIBCO). The hMPV-positive NPA sample was diluted in 2 ml of MEM without FBS and centrifuged at 200 × g for 5 min at 4° C to remove cellular debris. The resulting supernatant (referred to as NPA supernatant) was used as the viral source. Viral inoculum consisted of 150 µl of NPA supernatant plus 50 µl of infection medium (200 µl final volume). Vero cells were seeded in 24-well plates at a density adjusted to reach 70–80% confluence after 24 h of incubation in MEM. After this period, the monolayers were washed three times with PBS, and 200 µl of viral inoculum were added to each well. The plates were then centrifuged at 800 × g for 15 min at room temperature (RT). Afterwards, the plate was incubated at 37 °C and 5% CO_2 for 2 h, the monolayers were washed three times with PBS and 1 ml of infection medium per well was added. Cultures were observed daily for CPE by phase-contrast microscopy. At 4, 7, 10, 14, 17, and 21 days post-infection (dpi), the culture supernatants were collected and stored at − 70 °C until further analysis by PCR. After each collection, fresh infection medium was added to the monolayers to maintain the culture. This procedure was repeated over three successive blind passages, each lasting 21 days. CPE was observed only during the third passage. Positivity was confirmed by the presence of CPE and by RT-PCR targeting the hMPV N gene, as described below. The hMPV-positive culture supernatants obtained after this final passage were used as an infection inoculum for subsequent experiments.

RT-PCR

Total RNA was extracted from 140 µl of culture supernatants using the QIAamp® Viral RNA Mini Kit (Qiagen, GmbH, Hilden, Germany) following the manufacturer's instructions. RT-PCR for the detection of the hMPV N gene was performed to amplify a 199 bp fragment, using the Qiagen OneStep RT-PCR kit (Qiagen, Hilden, Germany). The conventional RT-PCR protocol was adapted from Bouscambert-Duchamp[35]. The following hMPV primers were used: Fw 5′-GTGATGCACTCAAGAGATACCC-3′ and Rv 5′- CATTGTTTGACCGGCC CCATAA-3′, at a final concentration of 50 µM each. Cycling conditions were as follows: 30 min at 50 °C and 15 min at 94 °C, followed by 40 cycles of 95 °C for 30 s, 58 °C for 30 s, and 72 °C for 1 min, with a final extension at 72 °C for 10 min. PCR products were separated by electrophoresis on a 1.5% agarose gel and visualized under UV light after ethidium bromide staining. This assay has an estimated sensitivity of ~ 10^2 copies/µl, as previously reported[17].

Indirect immunofluorescence assay

To visualize both the hMPV proteins and the actin network, Vero cells were seeded on glass coverslips at a density adjusted to reach at 60% confluence after 24 h. At different times post-infection, cells were washed three times with PBS, fixed with 4% paraformaldehyde and 120 mM sucrose (Sigma-Aldrich Laborchemikalien GmbH, Germany) for 20 min at RT and washed again with PBS. They were then permeabilized with 0.2% Triton™ X-100 (Sigma-Aldrich, St. Louis, MO) in PBS for 5 min at RT, followed by 3 washes with PBS for 5 min at RT, followed by 3 washes with PBS, and blocked with 5% bovine serum albumin (BSA, Sigma-Aldrich) in PBS, for 1 h at RT. To detect viral proteins, cells were incubated overnight at 4 °C with a mouse monoclonal anti-F protein/hMPV primary antibody (1:500; IMAGEN™ hMPV. Oxoid-Ltd.) diluted in 1% BSA/PBS. Although this antibody is provided as part of a direct immunofluorescence kit, in our protocol it was used within an indirect immunofluorescence assay, followed by incubation with a fluorescent-labeled secondary antibody to enhance signal intensity. After washing, samples were incubated with Alexa-Fluor 488-conjugated goat anti-mouse secondary antibody (1:1600; Thermo Fisher Scientific Inc., USA) for 1 h at RT. Actin filaments and nuclei were visualized using Phalloidin-Tetramethyl rhodamine-B (1:1000; Sigma-Aldrich) and Hoechst 1X (1 µg/ml; Thermo Fisher Scientific), respectively, for 1 h and 5 min at RT. Finally, coverslips were washed 3 times with PBS and mounted using Fluorsave (Calbiochem).

Sequence and phylogenetic analysis

The RT-PCR protocol was adaptaded from Van den Hoogen[36] to amplify a 696 bp fragment of the F gene, using the Qiagen OneStep RT-PCR kit (Qiagen, Hilden, Germany), with primers mix Fw 5′-CAATGCAGGTATAA

CACCAGCAATATC-3′ and Rv 5′-GCAACAATTGAACTGATCTTCAGGAAAC-3′, at a final concentration of 50 µM each. Cycling conditions were as follows: 30 min at 42 °C and 8 min at 95 °C, followed by 40 cycles of 94 °C for 1 min, 40 °C for 2 min and 72 °C for 3 min, and a final step of 72 °C for 10 min. The amplified products were separated by electrophoresis on a 1% agarose gel and visualized under UV light after ethidium bromide staining[17]. The PCR of 696 bp product was purified from a 1.5% agarose gel using the QIAquick Gel Extraction Kit (Qiagen, Germany) following the manufacturer's instructions. Nucleotide sequencing reactions were performed in both directions using the internal PCR primers and Sanger sequencing by Macrogen, Inc. (Seoul, Korea). Sequences were edited with MEGA-4.0.2 and aligned with sequences available in the GenBank, using the ClustalW. A Maximum Likelihood Phylogenetic Tree was generated using a 696 bp fragment of the fusion protein (F) gene, with PhyML 3.0 software (Université de Montpellier, France). Branch support was evaluated via non-parametric bootstrapping with 1000 pseudoreplicates. The nucleotide substitution model was choosen based on the AIC implemented in ModelTest-3.7 software (University of Vigo, Spain). The sequence was deposited in GenBank (accession no. MN117139).

Viral quantification by RT-qPCR

Viral RNA copies from supernatants obtained under different experimental conditions were determined by absolute quantification in an Applied Biosystems 7500 Fast-Real-time PCR system. The reaction mix was prepared by adapting the manufacturer's protocol for AgPath-ID™ One-Step RT-PCR Reagents (Applied Biosystems™): 2X RT-PCR Buffer = 1X; Forward and reverse PCR primers = 50 µM each; Syber Green (SYBR™ Green 10000X-Invitrogen) dilution 1/100 = 5.0 and − 5; 25X RT-PCR Enzyme Mix (ArrayScript™ Reverse Transcriptase and AmpliTaq Gold®DNA Polymerase) = 1X. The final volume was 25 µl, using 2.5 µl of viral RNA. Cycling conditions: 50 °C for 30 min; 45 cycles of 94 °C for 2 min, 95 °C for 10 s, 60 °C for 30 s and 72 °C for 30 s and a final step of 72 °C for 10 min. Data were analyzed in real-time using the Virtual Curve qPCR program from Applied Biosystems (Thermo Fisher Connect™). The viral load in each sample was calculated from a standard curve generated with serial dilutions (10^{-1} to 10^{-12}) of an hMPV N protein synthetic oligonucleotide (199 bp) (Ultramer® DNA Oligo) with a known concentration (6.0219×10^{13} copies of RNA/µl).

hMPV replication curve

Vero cells were grown at 60% confluence on glass coverslips (12 mm in 24-well plate) for 24 h and then infected with 200 µl of viral inoculum per well (1.97×10^{6} copies of RNA/µl; estimated molecular MOI: 3.3×10^{3} RNA copies/cell). The plates were centrifuged at 800 × g for 15 min at RT to facilitate viral adsorption. Afterwards, they were incubated at 37 °C with 5% CO_2 for 2 h. Then, the inoculum was removed, the monolayers were washed 3 times with PBS, and 1 ml of infection medium was added per well. This washing step ensured that any free viral particles from the inoculum were removed, so that subsequent detection of viral RNA in the supernatant reflects primarily newly synthesized viral progeny. The culture supernatants were harvested and the monolayers were fixed at different time points (8, 16, 24, 48, 72, and 96 hpi). Viral RNA was extracted from harvested supernatants using the QIAamp Viral RNA Mini Kit (Qiagen, GmbH, Hilden, Germany) following the manufacturer´s instructions. The extracted RNA was then employed for the detection and quantification of hMPV by Sybr (SYBR™ Green 10000×, Invitrogen) RT-qPCR (AgPath-ID™ One-Step RT-PCR Reagents, Applied Biosystems™). The mean number of copies of extracellular viral RNA/µl of culture supernatant was then calculated (Applied biosystems. Thermo-Fisher-Connect™).

Cells were processed for IF assay and the number of fluorescent dots/infected cell were calculated through the analysis of fluorescence images using the ImageJ-Fiji software (ImageJ 1.50c Wayne Rasband. NIH-USA).

Pharmacological treatment

Cell viability was evaluated after treatment with increasing concentrations of CytD (0.70, 1.25, 2.5, 5, and 10 µM) (Sigma-Aldrich, St. Louis, MO). After 24 h of treatment, cell viability was assessed using a colorimetric assay based on the reduction of a tetrazolium salt (2,3-bis[2-methyloxy-4-nitro-5-sulfophenyl]-2 H-tetrazolium-5-carboxanilide [XTT]) (Cell Proliferation Kit II, Roche/Sigma-Aldrich, St. Louis, MO, USA)[37]. A CytD concentration resulting in more than 90% cell viability [2.5 µM] was selected for subsequent experiments (Supplementary Fig. S1). The efficacy of CytD treatment was confirmed by Phalloidin staining and immunofluorescence analysis, which showed disorganization of the actin filaments and loss of their typical structure. Vero cells at 60% confluence cultured on glass coverslips were infected with hMPV according to the protocol described in the previous section. Infected cells were treated with CytD [2.5 µM] or vehicle (infection medium whitout CytD) during different phases of the replication cycle. CytD was diluted directly in the infection medium and added according to the experimental condition. Cells were exposed to CytD or vehicle either during the 2 h infection period, during the first 8 hpi (experimental period between 0 and 24 hpi), or during the first and the last 24 h (48–72 hpi) in an experimental period between 0 and 72 hpi. After each treatment period, the supernatant was removed, the cells were washed 3 times with PBS and fresh infection medium was added, according to each condition (Fig. 3B). Culture supernatants were used for RNA extraction and subsequent viral quantification by RT-qPCR, while the corresponding cell monolayers were processed for IF analysis.

Microscopy and digital image analysis

Immunostained cells were visualized using an inverted epi-fluorescence microscope (Olympus IX81, Olympus) and an inverted confocal microscope FV1000 (Olympus). Images were acquired with a CCD camera (Orca 1000, Hamamatsu-Corp.) using 40× and 60× oil immersion objectives. For each experimental condition, a minimum of ten random fields per coverslip were captured, covering at least 400 cells per time point. Quantification of intracellular infection was carried out by determining (i) the percentage of infected cells and (ii) the number of fluorescent dots per infected cell. Infection was defined by the presence of green fluorescence corresponding to

the F protein, and image analysis was performed using ImageJ-Fiji software. Data normalization was done by averaging the number of fluorescent dots per infected cell across all analyzed fields. Final images were assembled using Adobe Photoshop CS6 (Version 13.0.1.).

Statistical analysis

All tests and graphs were performed using GraphPad Prism 8.0 (GraphPad Software). Data represent results from at least three independent experiments, and values are presented as the mean ± standard error of the mean (SEM). Assumptions of homoscedasticity and normality were tested using Brown–Forsythe and Barlett´s tests and D´Agostino and Pearson test, respectively. All assumptions were met, allowing the use of Student's unpaired t-test or one-way ANOVA test for specific group comparisons. A significance level of $p < 0.05$ was considered statistically significant.

Data availability

The nucleotide sequence used in this work has been deposited in the GenBank repository (National Library of Medicine, NIH) under accession number [MN117139] and is publicly available at: https://www.ncbi.nlm.nih.gov/nuccore/MN117139.Additional data that support the findings of this study are available from the correspondi ng author [gpaglini@immf.uncor.edu] upon reasonable request.

Received: 21 November 2024; Accepted: 20 September 2025
Published online: 27 October 2025

References

1. Afonso, C. L. et al. Taxonomy of the order mononegavirales: Update 2016. *Arch. Virol.* **161**, 2351–2360 (2016).
2. Shafagati, N. & Williams, J. Human metapneumovirus—what we know now. *F1000Res* **7**, 1–11 (2018).
3. Kampmann, B. et al. Bivalent prefusion F vaccine in pregnancy to prevent RSV illness in infants. *N. Engl. J. Med.* **388**, 1451–1464 (2023).
4. Ballegeer, M. & Saelens, X. Cell-mediated responses to human metapneumovirus infection. *Viruses* **12**, 3–22 (2020).
5. Van Den Hoogen, B. G. et al. A newly discovered human pneumovirus isolated from young children with respiratory tract disease. *Nat. Med.* **7**, 719–724 (2001).
6. Sato, K. et al. Efficient isolation of human metapneumovirus using MNT-1, a human malignant melanoma cell line with early and distinct cytopathic effects. *Microbiol. Immunol.* **61**, 497–506 (2017).
7. Deffrasnes, C., Côté, S. & Boivin, G. Analysis of replication kinetics of the human metapneumovirus in different cell lines by Real-Time PCR. *J. Clin. Microbiol.* **43**, 488–490 (2005).
8. Li, M. et al. The host cytoskeleton functions as a pleiotropic scaffold: Orchestrating regulation of the viral life cycle and mediating host antiviral innate immune responses. *Viruses*. **15**, (2023).
9. Taylor, M. P., Koyuncu, O. O. & Enquist, L. W. Subversion of the actin cytoskeleton during viral infection. *Nat. Rev. Microbiol.* **9**, 427–439 (2011).
10. Shahriari, S., Wei, K. J. & Ghildyal, R. Respiratory syncytial virus matrix (M) protein interacts with actin in vitro and in cell culture. *Viruses* **10**, 7–12 (2018).
11. Kallewaard, N. L., Bowen, A. L. & Crowe, J. E. Cooperativity of actin and microtubule elements during replication of respiratory syncytial virus. *Virology* **331**, 73–81 (2005).
12. Mehedi, M. et al. Actin-related protein 2 (ARP2) and virus-Induced filopodia facilitate human respiratory syncytial virus spread. *PLoS Pathog.* **12**, 1–35 (2016).
13. Shahriari, S., Gordon, J. & Ghildyal, R. Host cytoskeleton in respiratory syncytial virus assembly and budding. *Virol. J.* **13**, 1–11 (2016).
14. El Najjar, F. et al. Human metapneumovirus induces reorganization of the actin cytoskeleton for direct Cell-to-Cell spread. *PLoS Pathog.* **12**, 1–30 (2016).
15. Gil, P. I. et al. Pixuna virus modifies host cell cytoskeleton to secure infection. *Sci. Rep.* **7**, 1–9 (2017).
16. Selden, L. A., Gershman, L. C. & Estes, J. E. A proposed mechanism of action of cytochalasin D on muscle actin. *Biochem. Biophys. Res. Commun.* **95**, 1854–1860 (1980).
17. Rodriguez, P. E. et al. Human metapneumovirus: epidemiology and genotype diversity in children and adult patients with respiratory infection in Córdoba, Argentina. *PLoS One*. **15**, e0244093 (2020).
18. Velez Rueda, A. J., Mistchenko, A. S. & Viegas, M. Phylogenetic and phylodynamic analyses of human metapneumovirus in Buenos Aires (Argentina) for a Three-Year period (2009–2011). *PLoS One*. **8**, 1–10 (2013).
19. Cifuentes-Munoz, N., Najjar, E., Dutch, R. E. & F. & Viral cell-to-cell spread: conventional and non-conventional ways. *Adv. Virus Res.* **108**, 85–125 (2020).
20. Ribó-Molina, P. et al. Human metapneumovirus infection of organoid-derived human bronchial epithelium represents cell tropism and cytopathology as observed in in vivo models. *Virology* **9**, 1–13 (2024).
21. Arnott, A. et al. Genetic variability of human metapneumovirus amongst an all ages population in Cambodia between 2007 and 2009. *Infect. Genet. Evol.* **15**, 43–52 (2013).
22. Kinder, J. T. et al. Respiratory syncytial virus and human metapneumovirus infections in three-dimensional human airway tissues expose an interesting dichotomy in viral replication, spread, and inhibition by neutralizing antibodies. *J. Virol.* **94**, 1–20 (2020).
23. Bernal, L. J., Velandia-Romero, M., Guevara, C. & Castellanos, J. E. Human metapneumovirus: laboratory methods for isolation, propagation, and plaque titration. *Intervirology* **61**, 301–306 (2019).
24. Tollefson, S. J., Cox, R. G. & Williams, J. V. Studies of culture conditions and environmental stability of human metapneumovirus. *Virus Res.* **151**, 54–59 (2010).
25. Jumat, M. R. et al. Imaging analysis of human metapneumovirus-infected cells provides evidence for the involvement of F-actin and the raft-lipid microdomains in virus morphogenesis. *Virol. J.* **11**, 1–12 (2014).
26. Nao, N. et al. Consensus and variations in cell line specificity among human metapneumovirus strains. *PLoS One*. **14**, 1–21 (2019).
27. Lee, H. et al. Improving pneumovirus isolation using a centrifugation and AZD1480 combined method. *J. Microbiol. Biotechnol.* **29**, 2006–2013 (2019).
28. Cox, R. G. et al. Human metapneumovirus is capable of entering cells by fusion with endosomal membranes. *PLoS Pathog.* **11**, 1–29 (2015).
29. Cifuentes-muñoz, N., Branttie, J., Slaughter, K. B. & Dutch, R. E. Human metapneumovirus induces formation of inclusion bodies for efficient genome replication and transcription. *J. Virol.* **91**, 1–18 (2017).
30. Geiser, J. et al. RSV and HMPV infections in 3D tissue cultures: mechanisms involved in Virus-Host and Virus-Virus interactions. *Viruses* **13**, 1–15 (2021).

31. Derdowski, A. et al. Human metapneumovirus nucleoprotein and phosphoprotein interact and provide the minimal requirements for inclusion body formation. *J. Gen. Virol.* **89**, 2698–2708 (2008).
32. Najjar, F. et al. Imaging analysis reveals budding of filamentous human metapneumovirus virions and direct transfer of inclusion bodies through intercellular extensions. *mBio* **14**, 1–18 (2023).
33. Merwaiss, F., Czibener, C. & Alvarez, D. E. Cell-to-cell transmission is the main mechanism supporting bovine viral diarrhea virus spread in cell culture. *J. Virol.* **93**, 1–18 (2018).
34. Boggs, K. B. et al. Human metapneumovirus phosphoprotein independently drives phase separation and recruits nucleoprotein to liquid-like bodies. *mBio* **13**, (2022).
35. Bouscambert-Duchamp, M. et al. Detection of human metapneumovirus RNA sequences in nasopharyngeal aspirates of young French children with acute bronchiolitis by real-time reverse transcriptase PCR and phylogenetic analysis. *J. Clin. Microbiol.* **43**, 1411–1414 (2005).
36. Van Den Hoogen, B. G., Osterhaus, D. M. E. & Fouchier, R. A. M. Clinical impact and diagnosis of human metapneumovirus infection. *Pediatr. Infect. Dis. J.* **23**, 25–32 (2004).
37. Jost, L. M., Kirkwood, J. M. & Whiteside, T. L. Improved short- and long-term XTT-based colorimetric cellular cytotoxicity assay for melanoma and other tumor cells. *J. Immunol. Methods*. **147**, 153–165 (1992).

Acknowledgements

We would like to thank Bernadette van den Hoogen for receiving PER in her laboratory and for advising on the viral isolation protocol; Guadalupe Carballal† and Cristina Videla for generously providing hMPV wild type positive control; Celia Frutos and Lucia Ghietto for technical assistance in Real Time RT-qPCR; Santiago Mirazo for generously providing polyclonal antibodies; Carlos Mas for technical assistance in confocal microscopy at the Centro de Micro y Nanoscopía de Córdoba, CEMINCO-CONICET-Universidad Nacional de Córdoba, Córdoba, Argentina. We particularly want to thank Miss Stella Ascheri for general technical assistance.

Author contributions

All authors were responsible for the study design. P.E.R., P.I.G. performed the experimental procedures and collected/curated data. P.E.R. and P.I.G. conducted statistical data analysis. P.E.R., P.I.G., A.C. and M.G.P. performed imaging analysis. J.C., A.C. and M.G.P. contributed ideas and comments. P.E.R., P.I.G., J.C., A.C. and M.G.P. interpreted the findings and drafted the manuscript. Supervision and project administration were done by A.C. and M.G.P. and funding's acquisition by M.G.P. and A.C. All authors have read and agreed to the published version of the manuscript.

Funding

This work was supported by grants from Secretaria de Ciencia y Tecnología-Universidad Nacional de Córdoba (SECYT-Consolidar-I Nº 336 20180100191CB to A.C. and SECYT-Consolidar-C Nº 33620180100091CB to M.G.P.) and from Fundación A. J. Roemmers (2018–2020 to A.C. and 2017–2019 to P.E.R). The funding sources had no involvement in the study design, data collection, analysis and interpretation, writing of the manuscript or in the decision to submit the article for publication.

Declarations

Competing interests

The authors declare no competing interests.

Additional information

Supplementary Information The online version contains supplementary material available at https://doi.org/10.1038/s41598-025-21385-9.

Correspondence and requests for materials should be addressed to M.G.P.

Reprints and permissions information is available at www.nature.com/reprints.

Publisher's note Springer Nature remains neutral with regard to jurisdictional claims in published maps and institutional affiliations.

Open Access This article is licensed under a Creative Commons Attribution-NonCommercial-NoDerivatives 4.0 International License, which permits any non-commercial use, sharing, distribution and reproduction in any medium or format, as long as you give appropriate credit to the original author(s) and the source, provide a link to the Creative Commons licence, and indicate if you modified the licensed material. You do not have permission under this licence to share adapted material derived from this article or parts of it. The images or other third party material in this article are included in the article's Creative Commons licence, unless indicated otherwise in a credit line to the material. If material is not included in the article's Creative Commons licence and your intended use is not permitted by statutory regulation or exceeds the permitted use, you will need to obtain permission directly from the copyright holder. To view a copy of this licence, visit http://creativecommons.org/licenses/by-nc-nd/4.0/.

© The Author(s) 2025